Earth Surf. Dynam. Discuss., 2, 733–772, 2014
www.earth-surf-dynam-discuss.net/2/733/2014/
doi:10.5194/esurfd-2-733-2014

Earth Surface Dynamics Discussions
Open Access

sedFlow – an efficient tool for simulating bedload transport, bed roughness, and longitudinal profile evolution in mountain streams

F. U. M. Heimann[1,2], D. Rickenmann[1], J. M. Turowski[3,1], and J. W. Kirchner[2,1]

[1]WSL Swiss Federal Institute for Forest, Snow and Landscape Research, 8903 Birmensdorf, Switzerland
[2]Department of Environmental System Sciences, ETH Zurich, 8092 Zurich, Switzerland
[3]Helmholtz Centre Potsdam, GFZ German Research Centre for Geosciences, Telegrafenberg, 14473 Potsdam, Germany

Received: 20 June 2014 – Accepted: 3 July 2014 – Published: 24 July 2014

Correspondence to: F. U. M. Heimann (florian.heimann@wsl.ch)

Published by Copernicus Publications on behalf of the European Geosciences Union.

Abstract

Especially in mountainuous environments, the prediction of sediment dynamics is important for managing natural hazards, assessing in-stream habitats, and understanding geomorphic evolution. We present the new modelling tool sedFlow for simulating fractional bedload transport dynamics in mountain streams. The model can deal with the effects of adverse slopes and uses state of the art approaches for quantifying macro-roughness effects in steep channels. Local grain size distributions are dynamically adjusted according to the transport dynamics of each grain size fraction. The tool sedFlow features fast calculations and straightforward pre- and postprocessing of simulation data. The model is provided together with its complete source code free of charge under the terms of the GNU General Public License (www.wsl.ch/sedFlow). Examples of the application of sedFlow are given in a companion article by Heimann et al. (2014).

1 Introduction

Environmental models typically seek to predict the future state of a system, based on information about its current state and the mechanisms that regulate its evolution through time. In the case of sediment transport by flowing water in open channels, the temporal evolution of these variables is determined by a complex interaction of multiple processes including hydraulic water routing, sediment entrainment, erosion and deposition. In recent years many numerical models have been developed for simulating sediment transport in rivers. However, most of these models are intended for, and only applicable in, lowland rivers with gentle slopes. In mountain streams the effects of macro-roughness and shear stress partitioning have to be considered. Otherwise, the sediment transport rates may be overestimated by several orders of magnitude (Rickenmann and Recking, 2011; Nitsche et al., 2011, 2012).

Few sediment transport models have been specifically designed for mountain streams. Cui et al. (2006) developed the two Dam Removal Express Assessment

ESURFD
2, 733–772, 2014

Models (DREAM-1&2), which are based on the previous models of Cui and Parker (2005) and Cui and Wilcox (2008) and which focus specifically on dam removal scenarios. Therefore the DREAM models feature the simulation of (a) bank erosion during the downcutting of reservoir deposits, (b) transcritical flow conditions, (c) combined bedload and suspended load transport, (d) the details of gravel abrasion, and (e) staged dam removal and partial dredging as options in the dam removal scenarios. Due to their specific focus, the wider applicability of the DREAM models is limited. Both the model of García-Martinez et al. (2006) or the model MIKE21C (DHI, 1999, with its modifications by Li and Millar, 2007) focus on a two-dimensional representation of hydraulic and sediment transport processes. Therefore, these models require more extensive input data and longer calculation times compared to one-dimensional model representations. As another example, the model of Papanicolaou et al. (2004) is intended for studying sediment transport under transcritical flow conditions by solving the unsteady form of the Saint–Venant equations, which results in long calculation times.

Other sediment transport models have been described by Mouri et al. (2011), Lopez and Falcon (1999) and Hoey and Ferguson (1994), which all feature the one dimensional simulation of fractional bedload transport using a simplified representation of the hydraulic processes. The model of Mouri et al. (2011) can represent a combination of debris flow, bedload and suspension load processes. In contrast, SEDROUT (Hoey and Ferguson, 1994) is designed to study the spatial and temporal evolution of local grain size distributions. Therefore, it determines the composition of the sediment surface layer by a numeric iteration within each time step. In its latest version, SEDROUT has been also extended to deal with islands and other features of river bifurcation (Verhaar et al., 2008). However, for none of the three models mentioned in this paragraph the source code, the executable model binary, or a detailed description of the model implementation is available.

The model Tom^{Sed} (formerly known as SETRAC) was developed to study the influence of different shapes of channel cross sections on bedload transport (Chiari et al., 2010; Chiari and Rickenmann, 2011). Therefore, the user can define cross sections

ESURFD
2, 733–772, 2014

with laterally varying bed elevations. The shape of a particular cross section stays the same during the complete simulation. Most published model applications used bedload transport calculations on a single grain size. In such a situation, all grain sizes and their spatial distribution are constant for the complete simulation. In this set up, Tom^{Sed} is slightly faster than real time in a typical application. A fractional transport approach with dynamic grain size distributions is implemented in Tom^{Sed} as well. However, it is rarely used due to the long calculation times.

The Topkapi model was originally developed as a rainfall–runoff model providing fast hydrologic simulations (Ciarapica and Todini, 2002). Later a sediment transport module was added, and this model version is called Topkapi ETH (Konz et al., 2011). The code is intended for the study of local-scale sediment transport in the context of large-scale hydrologic processes. Due to this scope of integrating different processes and scales, the model features a spatial as well as temporal subgridding approach. The hydrologic processes are simulated on a coarse two-dimensional grid with time steps that are an integer multiple of the time steps for the hydraulic and sediment transport processes. The latter two processes are simulated in a one-dimensional channel at a finer spatial resolution. This channel receives water from the hydrologic two-dimensional grid, but the morphodynamic changes due to bedload transport have no influence on the topography used for the hydrologic calculations. The channel cross section is represented by a rectangle and bedload transport is based on a single grain size approach, in which local grain-size distributions do not change over time. In typical applications, a flood event of several days can be simulated within a few minutes of calculation time.

Currently, no model is available that combines short calculation times with easy use and up-to-date sediment transport equations for alpine catchments. The new model sedFlow (Fig. 1) presented in this contribution has been developed to provide an efficient tool for the simulation of bedload transport in mountain streams. The following elements were important for the development of sedFlow:

1. provision of a sediment transport model together with its complete source code open and free of charge,

ESURFD
2, 733–772, 2014

2. implementation of state of the art approaches for calculating bedload transport in steep channels accounting for macro-roughness effects,
3. individual calculations for several grain diameter fractions (fractional transport),
4. consideration of the effects of adverse slopes in terms of ponding, e.g., due to sudden sediment deposition by debris flow inputs,
5. fast calculations for modelling entire catchments, and for automated calculation of multiple scenarios exploring a range of parameter space,
6. flexibility in model development featuring an object-oriented code design,
7. flexibility in model application featuring straightforward pre- and postprocessing of simulation data.

The model sedFlow thus fills a gap in the range of existing sediment transport models for mountain streams (Table 1) and the goals outlined above have led to the implementation described in the following sections. This implementation represents the current state of the model, and may be easily extended and adjusted in the future.

Detailed descriptions of examples of the application of sedFlow are given in a companion article by Heimann et al. (2014).

2 Implementation of the sedFlow model

2.1 Hydraulic calculation

Hydraulic equations describe the temporal evolution of the three-dimensional flow field of the water continuum. A formalised description of the involved processes has been provided by Navier and Stokes (given in the form for incompressible flow).

$$\rho\left(\frac{\delta(\boldsymbol{v})}{\delta t}+\boldsymbol{v}\cdot\nabla\boldsymbol{v}\right)=-\nabla p+\mu\nabla^2\boldsymbol{v}+\boldsymbol{f}; \quad (1)$$

ESURFD
2, 733–772, 2014

Here, ρ is fluid density, $\boldsymbol{v}$ is flow velocity, t is time, p is pressure and μ is dynamic viscosity. $\boldsymbol{f}$ summarises other influencing body forces. If large-scale backwater effects are not present, as is often the case in steep channels of mountain streams, the energy slope can be approximated by the bed slope (i.e. assumption of kinematic wave propagation) and the complete Navier–Stokes equation can be reduced to the following simplified, cross-section averaged form (e.g., Chow et al., 1988).

$$\frac{\delta Q}{\delta x} + \frac{\delta A}{\delta t} = Q_{\text{lat}} \tag{2}$$

Here, Q is discharge, x is distance in flow direction, A is wetted cross-sectional area and Q_{lat} is lateral water influx.

2.1.1 Flow routing

Within sedFlow a channel network joined by confluences can be simulated. At the upstream ends of the main channel and of each of the user-defined tributaries a discharge time series is input and has to be routed through the channel system. For the following discussion of hydraulic routing schemes we will differentiate between three cases: First, in *pondages*, the friction slope S_{f} is approximately zero ($S_{\text{f}} \approx 0$). Second, in *situations with parallel slopes*, the friction slope approximately equals the channel bed slope S_{b} ($S_{\text{f}} \approx S_{\text{b}}$), which is commonly true for steep S_{b}. Third, the *situations of moderate backwater effects* cover all cases between the extremes of pondages on the one hand and situations with parallel slopes on the other.

Especially in models not focussing on the details of the hydraulic routing, the kinematic wave approach (assuming the situation of parallel slopes) can be used based on a temporally explicit Eulerian forward approach (van de Wiel et al., 2007; Chiari et al., 2010). Such an approach can be used in sedFlow as well (see Sect. A1). However, Eulerian forward approaches must assume that all parameters within one timestep can be sufficiently approximated by their values at the beginning of the time step. In order to keep this assumption, Eulerian forward approaches require very small time steps,

ESURFD
2, 733–772, 2014

especially for fast processes. This can be problematic when a relatively fast process such as the routing of water is combined with a relatively slow process such as bedload transport including bed level adjustments. The water routing requires small timesteps and thus calculation times that may be orders of magnitude too long and slow from the perspective of bedload dynamics. Therefore, as an alternative, an implicit discharge routing is implemented in sedFlow as well. The implicit routing is unconditionally stable, and thus has no requirements concerning the length of time steps. In sedFlow the approach of Liu and Todini (2002) is used, which omits time consuming iterations and analytically finds the solution for the kinematic wave by a Taylor series approximation. However, the approach depends on a power law representation of discharge as a function of water volume in a reach. This means that it can only be applied to the specific cross-sectional shapes of an infinitely deep rectangular or v-shaped channels in combination with a power law flow resistance.

The kinematic wave assumption of parallel slopes is valid for steep channel gradients, which are typical of alpine catchments. Nevertheless, the kinematic wave assumption can be problematic especially in mountain streams, when tributaries deliver large amounts of sediment to the main channel within a relatively short time, e.g. during debris flow events. This may result in adverse slopes and backwaters in the main channel, violating the assumptions of a kinematic wave. In this case, sedFlow aborts simulations, whenever adverse slopes occur.

If it is necessary to deal with adverse slopes, one has to drop the kinematic wave approximation and use a backwater calculation instead. Unfortunately, the backwater calculation is numerically intensive. Therefore, within sedFlow, a pragmatic approach can be selected to deal with adverse slopes: Discharge is assumed to be uniform and thus equal along the entire channel only increasing at confluences for a given time step. This assumption of uniform discharge can be justified keeping in mind that the temporal scale for water routing is orders of magnitude smaller than the temporal scale for morphodynamics. In the case of positive slopes, flow depth and velocity are commonly calculated using the bed slope as proxy for the friction slope and thus assuming

ESURFD
2, 733–772, 2014

parallel slopes. However, they may be adjusted to remain below a maximum Froude number. In cases of adverse slopes, the formation of pondages is simulated. That is, flow depth and velocity are selected in a way to ensure a minimum gradient of hydraulic head, which is (a) positive and (b) close to zero and thus (a) ensures numeric stability and (b) approximately corresponds to the hydraulic gradient of a pondage. For bedload transport calculations the gradient of the hydraulic head is used, which by definition can only have positive slopes. Thus, the energy slope for bedload transport estimation is *not* the result of a backwater calculation, but it is the gradient between individual hydraulic head values, which under normal conditions have been calculated independent from each other using the local bed slope as a proxy for friction slope. This approach is based on the assumption that the simulated system only consists of the two extreme cases of pondages on the one hand and situations of parallel slopes on the other. At a spatial discretisation of several tens of metres, the assumption of the two extreme cases is valid for many mountain streams and it provides for the efficient simulation of pondages, by omitting numerically extensive backwater calculations. However, it has to be noted that this approach will produce large errors when intermediate cases of moderate backwater effects are part of the simulated system. In such systems, the first approach, which uses bed slope both as friction slope for the hydraulic calculations and as energy slope for the sediment transport calculations, will produce better estimates of the transported sediment volumes, but requires the absence of adverse channel gradients.

Heimann et al. (2014) have demonstrated that despite their simplicity the implemented hydraulic concepts (Fig. 2) appear to be sufficient for a realistic integrated representation of bedload transport processes, in that very similar results are obtained for the different hydraulic routing schemes described above.

2.1.2 Flow resistance

The interaction of flowing water with the structures of the river bed and banks determines the relation between the average downstream velocity and the wetted cross

ESURFD
2, 733–772, 2014

section area, the product of which is discharge. This interaction is summarised as flow resistance, which can be described by the following physically based relation:

$$\sqrt{\frac{8}{f}} = \frac{v}{\sqrt{g \cdot r_\mathrm{h} \cdot S_\mathrm{f}}} \tag{3}$$

Here, f is the Darcy–Weisbach friction factor, v is cross-sectional mean flow velocity, g is gravitational acceleration and r_h is hydraulic radius. The flow routing method of Liu and Todini (2002) requires a power-law relation between discharge and water volume within a reach. Therefore the following flow resistance law can be used in sedFlow.

$$\sqrt{\frac{8}{f}} = j_1 \cdot \left(\frac{r_\mathrm{h}}{k \cdot D_x}\right)^{l} \tag{4a}$$

$$\sqrt{\frac{8}{f}} = 6.5 \cdot \left(\frac{r_\mathrm{h}}{D_{84}}\right)^{\frac{1}{6}} \tag{4b}$$

Here, j_1, k and l are empirical constants and D_x is the xth percentile diameter of the local grain size distribution. Selecting $l = \frac{1}{6}$, this formula represents a classic grain-size-dependent Gauckler–Manning–Strickler relation. For the other variables, the values $j_1 = 6.5$, $k = 1$ and $x = 84$ (Eq. 4b) have been found to perform well in reproducing observational data for deeper flows with $\frac{r_\mathrm{h}}{D_{84}}$ larger than about 7–10 (Rickenmann and Recking, 2011). If another flow routing is used, one can select the variable power equation flow resistance approach provided by Ferguson (2007) with the parameter values proposed by Rickenmann and Recking (2011), which was recommended also for the application in steep channels including shallow flows with small relative flow depths $\frac{r_\mathrm{h}}{D_{84}}$.

$$\sqrt{\frac{8}{f}} = \frac{j_1 \cdot j_2 \cdot \frac{r_\mathrm{h}}{D_{84}}}{\sqrt{j_1^2 + j_2^2 \cdot \left(\frac{r_\mathrm{h}}{D_{84}}\right)^{\frac{5}{3}}}}; \quad \text{with } j_1 = 6.5 \text{ and } j_2 = 2.5 \tag{5}$$

ESURFD
2, 733–772, 2014

In general, flow resistance describes the interaction between the water flow and the bed, consisting of the resistance offered to the flow and the drag forces exerted on the bed and its structures. A part of this drag, namely the skin drag, is responsible for the transport of sediment grains (e.g., Morvan et al., 2008). The residual parts of the drag exerted on surface geometries such as bed forms and channel shape features (e.g. bends and irregular channel width) may be summarised as form or macroroughness. In other terms, the form roughness reduces the energy available for the transport of sediment. If macrorougness is not accounted for in steep channels, this may lead to a considerable overestimation of bedload transport capacity (Rickenmann, 2001, 2012; Yager et al., 2007; Badoux and Rickenmann, 2008; Chiari and Rickenmann, 2011; Nitsche et al., 2011, 2012; Yager et al., 2012). To correct for form roughness, Nitsche et al. (2011) suggested to introduce a reduced energy slope, which represents a fraction of the real gradient, and which is based on a flow resistance partitioning approach of Rickenmann and Recking (2011) and Nitsche et al. (2011).

$$S_{\mathrm{red}} = S \cdot \left(\frac{f_0}{f_{\mathrm{tot}}}\right)^{0.5 \cdot e} = S \cdot \left[\frac{2.5 \cdot \left(\frac{r_{\mathrm{h}}}{D_{84}}\right)^{\frac{5}{6}}}{\sqrt{6.5^2 + 2.5^2 \cdot \left(\frac{r_{\mathrm{h}}}{D_{84}}\right)^{\frac{5}{3}}}}\right]^{e} \quad (6)$$

Here, S_{red} is the reduced slope to account for macroroughness effects, S is channel or hydraulic energy slope, f_0 is base-level flow resistance according to Eq. (4b), f_{tot} is total flow resistance according to Eq. (5) and e is an exponent ranging from 1 to 2, with a typical value of e = 1.5.

2.2 Bedload transport calculation

2.2.1 Bedload transport rate

Several methods for the calculation of bedload transport capacity are implemented in sedFlow: Sects. A2 to A6 describe the method of Cheng (2002) based on flume data,

ESURFD
2, 733–772, 2014

the method of Wilcock and Crowe (2003) based on flume data, the method of Recking (2010) based on field observations, and the method of Rickenmann (2001) based on flume data, together with its simplified version and its version based on discharge instead of shear stress. The method of Rickenmann (2001) was tested together with Eq. (6) with bedload transport observations in steep mountain streams (Nitsche et al., 2011). The equations of Wilcock and Crowe (2003) have been derived from fractional bedload transport data. The equation of Recking (2010) was developed for the estimation of total bedload transport rates.

In the same way as the equations of Meyer-Peter and Müller (1948), Fernandez Luque and van Beek (1976) and Soulsby and Damgaard (2005), the equation of Rickenmann (2001) (Sect. A5; especially its simplified version in Eq. A21) is a good example for the following generic type of bedload estimation methods.

$$\Phi_b = a \cdot \theta^b \cdot (\theta - \theta_c)^d \tag{7}$$

Here, $\Phi_b = \frac{q_b}{\sqrt{(s-1)gD^3}}$ is dimensionless bedload flux, θ is dimensionless bed shear stress, θ_c is dimensionless bed shear stress threshold for the initiation of motion, q_b is bedload flux per unit flow width, D is grain diameter, a, b and d are empirical constants, and $s = \frac{\rho_s}{\rho}$ is the density ratio of solids ρ_s and fluids ρ. In such a type of equation, bedload transport is mainly a power law of the fraction of the dimensionless bed shear stress which exceeds some threshold for the initiation of bedload motion. This threshold is known as the Shields criterion (Shields, 1936) with values ranging from 0.03 to 0.05. In natural channels complexity and thus energy losses increase at steep bed slopes S_b. Therefore, Lamb et al. (2008) suggested the following empirical relation to account for increasing θ_c values with increasing S_b.

$$\theta_c = 0.15 \cdot S_b^{0.25} \tag{8}$$

As the application of Eq. (8) may result in too small thresholds for gentle slopes, a minimum Shields value is introduced. In sedFlow, either a constant threshold or

ESURFD
2, 733–772, 2014

a slope-dependent threshold according to Eq. (8) combined with a minimum value, can be used.

The estimated bedload flux can be corrected for gravel abrasion according to the classic equation of Sternberg (1875), in which $q_{b_{abr}}$ is bedload flux per unit flow width corrected for abrasion, λ is an empirical abrasion coefficient and ΔX is the travel distance of the grains. Here, the material loss due to erosion is regarded as suspension throughput load.

$$q_{b_{abr}} = q_b \cdot \exp(-\lambda \cdot \Delta X) \tag{9}$$

If grain size fractions are treated individually, the calculated bedload capacity Φ_b needs to be normalised with F_i, the relative portion of bed surface material of a grain size fraction i, compared to the total surface material with $D > 2\,\mathrm{mm}$. Here, F_i can be interpreted as the availability of a certain grain size fraction in the bed. For an example see Eq. (A24) in Sect. A7 compared to Eq. (A20) in Sect. A5. Additionally, further details have to be accounted for, such as the varying exposure of different grain size fractions, grain-size-dependent grain-grain interactions and so on. This is commonly done using some sort of hiding function. Even though it focuses mainly on grain exposure, a hiding function is used to integrate all kinds of grain size-dependent-effects which are not covered by the capacity estimation methods. Within sedFlow a relatively simple power-law hiding function can be used (Parker, 2008)

$$\theta_{ci} = \theta_c \cdot \left(\frac{D_i}{D_x}\right)^m \tag{10}$$

as well as the one by Wilcock and Crowe (2003).

$$\theta_{ci} = \theta_c \cdot \left(\frac{D_i}{D_m}\right)^{m_{wc}} \quad \text{with} \quad m_{wc} = \frac{0.67}{1 + \exp\left(1.5 - \frac{D_i}{D_m}\right)} - 1 \tag{11}$$

ESURFD
2, 733–772, 2014

Here, θ_{ci} is the θ_c for the ith grain size fraction, D_i is the mean grain diameter for ith grain size fraction, m is an empirical hiding exponent, D_m is the geometric mean diameter of the local grain size distribution and m_wc is the hiding exponent according to Wilcock and Crowe (2003). The empiric exponent m ranges from 0 to −1, where $m = -1$ corresponds to the case, in which the value of $(\theta - \theta_c)$ is independent of the grain size fraction diameter D_i, and $m = 0$ corresponds to no influence by hiding at all. For $x = 50$, the values for m, which have been derived from various field observations, typically vary within a range from −0.60 to −1.00 (Recking, 2009) and unfortunately there are only few data points for $D_i > D_{50}$.

For consistency, the following $\theta_{ci,\mathrm{r}}$ is used in bedload transport calculations.

$$\theta_{ci,\mathrm{r}} = \theta_{ci} \cdot \gamma \tag{12}$$

Within sedFlow two alternatives are implemented for the calculation of the correction factor γ:

$$\gamma = \frac{S_\mathrm{red}}{S} \tag{13a}$$

$$\gamma = \frac{S_\mathrm{c}}{S} \tag{13b}$$

In the first approach (Eq. 13a), $\theta_{ci,\mathrm{r}}$ varies with discharge, as it depends on S_red, which in turn is a function of r_h. In the second approach (Eq. 13b) suggested by Nitsche et al. (2011), $\theta_{ci,\mathrm{r}}$ is independent of discharge. The value of S_c is calculated using Eq. (6), with the value of r_h replaced by the critical hydraulic radius $r_{\mathrm{h,\,c}}$:

$$r_{\mathrm{h,\,c}} = \theta_c \cdot \left(\frac{\rho_\mathrm{s}}{\rho} - 1\right) \cdot D_{50} \cdot \frac{1}{S} \tag{14}$$

Good arguments can be found for both approaches. Due to the lack of suitable data, it is hard to decide which approach is more plausible.

ESURFD
2, 733–772, 2014

2.2.2 Evolution of channel bed slope

The temporal evolution of the longitudinal profile is simulated in sedFlow based on a finite-difference version of the general Exner equation (e.g., Parker, 2008).

$$(1 - \eta_{\text{pore}}) \cdot \frac{\delta z}{\delta t} + \frac{\delta q_{\text{b}}}{\delta x} + q_{\text{b}_{\text{lat}}} = 0 \quad (15)$$

Here, η_{pore} is pore volume fraction, z is elevation of channel bed and $q_{\text{b}_{\text{lat}}}$ is lateral bedload influx per unit flow width. Eq. (15) allows calculating the new channel slope $\frac{\Delta z}{\Delta x}$ after each time step. Up to now, infinitely deep rectangles are used within sedFlow as the shape of the cross-sectional profiles, with the complete width defined as active width (i.e. sediment transport takes place over the complete width).

All three elements, the cross-sectional channel geometry, its alteration due to morphodynamics and the determination of the active width are implemented as abstract classes. Thus, the presented realisations just represent some current state of the code and any programmer can easily extend the code to deal with more complex cross-sectional geometries. However, the implicit flow routing by Liu and Todini (2002), with its advantages in terms of simulation efficiency, requires infinitely deep rectangular or v-shaped channels (together with a simple power equation flow resistance law such as Eq. 4a).

Additionally Stephan (2012) has studied the impact of the rectangular shape approximation and found that at least during major flood events it is negligible compared to the other uncertainties. Stephan (2012) recalculated bedload transport with Tom$^{\text{Sed}}$ for the August 2005 transport event in the catchments of the Chiene, Chirel and Schwarze Lütschine. For details on the catchment and event characteristics see Chiari and Rickenmann (2011). The simulations were repeated once with a detailed channel geometry as presented in Chiari and Rickenmann (2011) and twice with a rectangular substitute channel. The width of the rectangular substitute channels w was determined based on a discharge Q_{rep}, which is representative for the simulation period. The channel width was selected to produce the same wetted cross-sectional area and hydraulic radius for

ESURFD
2, 733–772, 2014

the representative discharge as was simulated for the detailed channel geometry. In one approach the threshold discharge for the initiation of bedload motion Q_c and the maximum discharge of the simulation period Q_{max} were averaged to find Q_{rep}, for which the representative channel width was determined. In the second approach, one width w was determined for both Q_c and Q_{max} and then the two widths were averaged to find the representative channel width. The detailed channel geometry did not produce much different results than the rectangular substitutes when compared with the field observations on bedload transport (Fig. 3). For further details see Stephan (2012).

Finally, the introduction of more complex cross-sectional shapes raises the question of how these shapes are influenced and altered through morphodynamics. As far as we know, no generally accepted concepts are available for this problem.

2.3 Grain size distribution changes

In sedFlow the alluvial substrate of the river is represented by a stack of horizontal layers with homogeneous grain size characteristics. The topmost layer of the bed is the platform for the interaction between bed and flow and it is typically called the active layer. The grain size distribution of the active layer is used for the determination of the flow resistance, hiding processes and the bedload transport capacity (Fig. 1). All deposited material is added to this layer; all eroded material is taken from it. The thickness of this layer determines the inertia of its evolving grain size distribution. When the alluvium thickness gets very thin, the shape properties of bedrock are used to determine flow resistance and hiding. The thickness of the active layer may be set constant or dynamic as a multiple of some grain size percentile. Three different approaches are available within sedFlow for the interaction between the active layer and the underlying subsurface alluvium.

The first method (Fig. 4) has been adapted from the one described by van de Wiel et al. (2007). A lower and upper threshold are defined for the thickness of the active layer. Whenever these thresholds are exceeded, sediment increments are incorporated from or released to the subsurface alluvium underneath until the active layer thickness

ESURFD
2, 733–772, 2014

again takes a value within the given thresholds. The sediment increments are stored as bed strata underneath the active layer. In this way the simulated river bed is able to remember its history. In contrast to the procedure of van de Wiel et al. (2007) the thickness of the sediment increments can be defined independently of the thickness of the active layer. Trivially, the thickness of the increments defines the minimum distance between the thresholds for the active layer thickness. The smaller this distance between the thresholds is, the more intense is the interaction between the active layer and the underlying subsurface alluvium.

The second approach (Fig. 5), which has been applied in various models (e.g., Hunziker, 1995), can be described as an extreme case of the first one, in which the two thresholds collapse to a single target thickness for the active layer. In this case, any addition or removal of material to or from the active layer is instantaneously balanced against the underlying subsurface alluvium. In this case of maximum interaction between active layer and subsurface alluvium, the subsurface alluvium is represented by one homogenised volume without any internal structure. The target thickness is usually determined at the start of a simulation and then kept constant. Alternatively, it can be dynamically adjusted based on a Eulerian forward approach, in which the thickness is updated at the end of each time step.

The third approach (Fig. 6) is a variation of the second one. When sediment is eroded, only the volume of the active layer is instantaneously replaced from the subsurface, while the grain size distribution stays the same. The sediment volume that is transported from the subsurface alluvium to the active layer shares the grain size distribution of the subsurface alluvium only if a condition for the break-up of an armouring layer is fulfilled:

$$\theta_{50} \geq \theta_{c\mathrm{a}} \tag{16}$$

Here, θ_{50} is a representative dimensionless shear stress θ for the median diameter D_{50} of the active layer and $\theta_{c\mathrm{a}}$ is a representative θ_c for the active layer. To avoid artefacts due to a hard threshold, some fraction i_s of the sediment transported from the

ESURFD
2, 733–772, 2014

subsurface alluvium to the active layer has the grain size distribution of the subsurface alluvium already before the break-up condition is fulfilled. The rest $(1 - i_s)$ has the grain size distribution of the active layer:

$$i_s = \frac{\theta_{50} - \theta_{cs}}{\theta_{ca} - \theta_{cs}} \quad \text{with} \quad 0 \le i_s \le 1 \quad \text{and} \quad 0 < \theta_{cs} < \theta_{ca} \tag{17}$$

Here, i_s is the relative grain size influence from the subsurface alluvium and θ_{cs} is a representative θ_c for the subsurface alluvium. The value of θ_{cs} can be estimated, e.g., according to Eq. (8), while the value of θ_{ca} can be estimated using the following relation according to Jäggi (1992):

$$\theta_{ca} = \theta_{cs} \cdot \left(\frac{D_{\mathrm{mArith_a}}}{D_{\mathrm{mArith_s}}} \right)^{\frac{2}{3}} \tag{18}$$

Here, $D_{\mathrm{mArith_a}}$ and $D_{\mathrm{mArith_s}}$ are the arithmetic mean diameters of the grain size distribution of a the active layer and of s the subsurface alluvium.

For non-fractional studies, the active layer concept can be turned off. In that case, the complete alluvium is represented by a single homogeneous layer, which directly interacts with the flow.

3 Discussion

In the following subsections, various details of the implementation of sedFlow are discussed and compared to implementations in similar models. Differences are explained in the context of the differing scopes of the respective models.

3.1 Fractional transport and grain size distributions

sedFlow is optimised for the simulation of fractional bedload transport, in order to study dynamically adjusting grain size distributions and their effects on hydraulics and

ESURFD
2, 733–772, 2014

bedload transport together with the effects of an evolving channel slope. In this context, different concepts are provided for the interaction between the active surface layer and the underlying alluvium. As grain size distributions will dynamically adjust to be consistent with the local circumstances (channel width, slope, etc.), this numeric concept might have the potential to partially compensate the uncertainty related to local grain size distribution data. For a more detailed discussion of this topic see Heimann et al. (2014).

Within Topkapi ETH fractional transport is not implemented and within Tom^{Sed} it is rarely used due to long calculation times. These models have a different application objective, for which dynamic grain size distributions are of subordinate relevance.

The approach of Lopez and Falcon (1999) for the evolution of the local grain size distribution is similar to the approach of the threshold-based layer interaction (Fig. 4) within sedFlow. However, Lopez and Falcon (1999) only introduced a lower threshold for the thickness of the active layer. This means that the subsurface alluvium remains constant even in cases of massive aggradation and that the active layer may reach unrealistically high thickness values, especially in cases of intense aggradation.

In SEDROUT, the surface layer grain size distribution is determined as a function of the spatial derivative of fractional transport rates and the thickness of the surface layer, which in turn is a function of the surface layer grain size distribution. This set of equations is solved by numeric iteration within each time step. In sedFlow, this numerically extensive procedure is replaced by a constant surface layer thickness or an Eulerian forward approach, in which the layer thickness is updated at the end of each time step. These more pragmatic approaches have been selected because fast simulations are one of the main aims of sedFlow.

3.2 Adverse slopes

Within sedFlow adverse slopes and their effects in terms of pondages can be considered using uniform discharge hydraulics. This approach is based on the assumption that the simulated system only consists of the two extreme cases of pondages on the

ESURFD
2, 733–772, 2014

one hand and situations of parallel slopes on the other. This assumption is valid in many mountain streams and it allows for fast simulations, which have been another main objective for the development of sedFlow. However, in the intermediate case of moderate backwater effects, it may produce large errors. The implemented approach corresponds to the situation of a confined channel, in which the sudden deposition of large volumes of sediment e.g. by debris flow inputs may produce pondages.

Within Topkapi ETH any large volumes of deposited material, which would produce adverse slopes, are instantaneously distributed to downstream river reaches until all slopes are positive. This algorithm would correspond to instantaneous landslides within the channel or to debris flows with short travel distances, but such phenomena are typically not observed in mountain streams. However, intantaneous lateral sediment input is not the main focus of the Topkapi ETH model. In the context of its intended applications, the described algorithm of Topkapi ETH is an appropriate pragmatic approach to conserve mass and ensure positive bed slopes, which are used as energy slopes in the implemented kinematic wave approach.

Within Tom^{Sed} any deposited material, which would produce adverse slopes, is fed to a virtual sediment storage, which does not contribute to elevation changes in the main channel. As long as there is sediment in this virtual storage, any erosion or deposition is applied to this storage keeping the main channel untouched. That means that the elevation of the main channel is frozen as long as there is material in the virtual storage. In some way this algorithm corresponds to a lateral displacement of the river channel due to large volumes of deposited material, which is stored next to the new channel. However, in mountain rivers the amount of material that is fed from the deposits to the main channel depends on the stability of the deposit slopes. Therefore, the new channel may well lower its elevation due to erosion, even if there is still some material in storage next to the channel. However, the situation of lateral channel displacement is close to the limits of a one-dimensional simulation and the described algorithm of Tom^{Sed} ensures positive bed slopes (used as proxy for the energy slopes)

ESURFD
2, 733–772, 2014

in a way which corresponds to some extent to a natural process, even though it violates conservation of mass within the main channel.

3.3 Simulation speed

Besides the selection of the coding language C++, for which there are powerful compilers available, we have implemented a spatially uniform discharge within each segment of the channel network, as well as an implicit kinematic wave flow routing approach, both aimed at providing a modelling tool for fast simulations. Both hydraulic approaches allow for coarse temporal discretisations and the implemented algorithm of Liu and Todini (2002) omits computationally demanding iterations. The ideal temporal discretisation (as fine as necessary and as coarse as possible) can be obtained from the Courant–Friedrichs–Lewy (CFL) criterion based on the speed of bedload (multiplied by a user defined safety factor). As a result, several years of bedload transport and resulting slope and grain size distribution adjustment can be simulated with sedFlow within only few hours of calculation time on a regular 2.8 GHz central processing unit (CPU) core.

In Topkapi ETH the implicit kinematic wave flow routing is also implemented using the algorithms of Liu and Todini (2002). However the length of the time steps used for the bedload transport simulations may differ from the ideal length, as it is defined as an integer multiple of the time steps used for the hydrologic simulations. This implementation is due to Topkapi ETH's aim to simulate different processes at different scales.

Within Tom^{Sed}, explicit kinematic wave flow routing is implemented. Thus, time steps need to be determined using the CFL criterion based on water flow velocity. Therefore, time steps are shorter than in sedFlow or Topkapi ETH and slow down the simulations considerably. The choice of the explicit water flow routing is due to Tom^{Sed}'s aim to simulate the effects of the shape of channel cross sections. The implicit flow routing based on the algorithms of Liu and Todini (2002) requires simple rectangular or v-shaped channels and would therefore prevent any detailed study of channel geometry.

ESURFD
2, 733–772, 2014

3.4 Flexibility

To ensure flexibility of application, we selected regular spreadsheets as the file format for the data input to sedFlow. Thus preprocessing can be done with common software applications, which are familiar to most users, so that data from any study catchment can be quickly and easily prepared for a sedFlow simulation. This contrasts with Tom^{Sed}, which uses the extensible markup language (xml) file format for data input, as well as with Topkapi ETH, which partially requires *Matlab* preprocessing. In sedFlow different equation sets can be selected and combined by the user for the main process representations (flow routing, flow resistance, initiation of bedload motion, transport capacity, etc.). The number, content and format of the output files can be defined by the user as well, in order to get the best solution for the respective study objectives.

To ensure flexibility of model development we selected an object-oriented design for the internal structure of the sedFlow code. In such a code, succeeding programmers just create new realisations for predefined code-interfaces without revising the model core. It is not necessary to know (virtually) anything about the model itself. The only piece of code that the programmer will have to read is the specification of the relevant code interface, which is typically not longer than two printout pages.

4 Conclusions

The new model sedFlow complements the range of existing tools for the simulation of bedload transport in steep mountain streams. It is an appropriate tool if (I) grain size distributions need to be dynamically adjusted in the course of a simulation, if (II) the effects of pondages e.g. due to debris flow inputs might play a role in the study catchment or if (III) one simply needs a fast simulation of bedload transport with quick and easy pre- and post-processing. Detailed descriptions of examples of the application of sedFlow are given in a companion article by Heimann et al. (2014).

ESURFD
2, 733–772, 2014

The current version of the sedFlow code and model can be downloaded under the terms of the GNU General Public License (GPL) at the following web page: www.wsl.ch/sedFlow.

Appendix A: Supplementary methods

A1 Explicit hydraulics

$$\frac{\delta V}{\delta t} = Q^{\mathrm{u}}_{T-1} - Q_{T-1}; \tag{A1}$$

$$V_T = V_{T-1} + \left(\frac{\delta V}{\delta t} \cdot \Delta t\right); \tag{A2}$$

$$r_{\mathrm{h}T} = \mathrm{geom}(V_T); \tag{A3}$$

$$Q_T = \mathrm{fr}\left(r_{\mathrm{h}T}\right); \tag{A4}$$

A2 Bedload capacity estimation according to Cheng (2002), modified for fractional transport

$$\Phi_{\mathrm{bi}} = \beta \cdot \theta^{1.5}_{i,\mathrm{r}} \cdot \exp\left(-\frac{\theta_{ci,\mathrm{r}}}{\theta^{1.5}_{i,\mathrm{r}}}\right); \quad \text{with} \quad \beta = 13 \tag{A5}$$

$$\text{and} \quad \Phi_{\mathrm{bi}} = \frac{q_{\mathrm{bi}}}{F_i\sqrt{(\frac{\rho_{\mathrm{s}}}{\rho} - 1)gD^3_i}} \quad \text{and} \quad q_{\mathrm{b}} = \Sigma q_{\mathrm{bi}};$$

A3 Bedload capacity estimation according to Wilcock and Crowe (2003)

$$v^* = \sqrt{\frac{\tau}{\rho}}; \tag{A6}$$

ESURFD
2, 733–772, 2014

$$m_{\mathrm{wc}} = \frac{0.67}{1 + \exp\left(1.5 - \frac{D_i}{D_{\mathrm{m}}}\right)} - 1; \tag{A7}$$

$$\frac{\tau_{\mathrm{r}}}{\tau_{\mathrm{rm}}} = \left(\frac{D_i}{D_{\mathrm{m}}}\right)^{m_{\mathrm{wc}}+1}; \tag{A8}$$

$$\tau^*_{\mathrm{rm}} = 0.021 + \left[0.015 \cdot \exp\left(-20 F_{\mathrm{s}}\right)\right] \tag{A9}$$

$$\tau_{\mathrm{rm}} = \tau^*_{\mathrm{rm}} \cdot \rho \cdot g \cdot D_{\mathrm{m}} \cdot \left(\frac{\rho_{\mathrm{s}}}{\rho} - 1\right); \tag{A10}$$

$$W^* = 0.002 \cdot \left(\frac{\tau}{\tau_{\mathrm{r}}}\right)^{7.5} \quad \text{for} \quad \frac{\tau}{\tau_{\mathrm{r}}} < 1.35; \tag{A11}$$

$$W^* = 14 \cdot \left[1 - \frac{0.894}{\sqrt{\frac{\tau}{\tau_{\mathrm{r}}}}}\right]^{4.5} \quad \text{for} \quad \frac{\tau}{\tau_{\mathrm{r}}} \geq 1.35; \tag{A12}$$

$$q_{\mathrm{b}} = F_i \cdot \frac{W^* \cdot v^{*3}}{\left(\frac{\rho_{\mathrm{s}}}{\rho} - 1\right) \cdot g}; \tag{A13}$$

A4 Bedload capacity estimation according to Recking (2010)

$$\theta_{c84} = (1.32 \cdot S + 0.037) \cdot \left(\frac{D_{84\mathrm{surf}}}{D_{50\mathrm{surf}}}\right)^{-0.93}; \tag{A14}$$

$$L = 12.53 \cdot \left(\frac{D_{84\mathrm{surf}}}{D_{50\mathrm{surf}}}\right)^{4.445\sqrt{S}} \cdot \theta_{c84}^{1.605}; \tag{A15}$$

$$\theta_{84} = \frac{\tau}{(\rho_{\mathrm{s}} - \rho) \cdot g \cdot D_{84\mathrm{surf}}}; \tag{A16}$$

ESURFD
2, 733–772, 2014

$$\Phi_b = 0.0005 \cdot \left(\frac{D_{84surf}}{D_{50surf}}\right)^{-18\sqrt{S}} \cdot \left(\frac{\theta_{84}}{\theta_{c84}}\right)^{6.5} \quad \text{for} \quad \theta_{84} < L; \tag{A17}$$

$$\Phi_b = 14 \cdot \theta_{84}^{2.45} \quad \text{for} \quad \theta_{84} \geq L; \tag{A18}$$

$$q_b = \Phi_b \cdot \sqrt{\left(\frac{\rho_s}{\rho} - 1\right) \cdot g \cdot D_{84surf}^3}; \tag{A19}$$

A5 Bedload capacity estimation according to Rickenmann (2001) based on θ

$$\Phi_b = 3.1 \cdot \left(\frac{D_{90}}{D_{30}}\right)^{0.2} \cdot \sqrt{\theta} \cdot (\theta - \theta_c) \cdot \mathrm{Fr} \cdot \frac{1}{\sqrt{\frac{\rho_s}{\rho} - 1}} \tag{A20}$$

Equation (A20) may be simplified using the mean experimental value of $\left(\frac{D_{90}}{D_{30}}\right)^{0.2} = 1.05$ and a common value of $\frac{\rho_s}{\rho} = 2.65$:

$$\Phi_b = 2.5 \cdot \sqrt{\theta} \cdot (\theta - \theta_c) \cdot \mathrm{Fr} \tag{A21}$$

A6 Bedload capacity estimation according to Rickenmann (2001) based on q

$$q_b = 3.1 \cdot \left(\frac{\rho_s}{\rho} - 1\right)^{-1.5} \cdot \left(\frac{D_{90}}{D_{30}}\right)^{0.2} \cdot (q - q_c) \cdot S^{1.5}; \tag{A22}$$

$$q_c = 0.065 \cdot \left(\frac{\rho_s}{\rho} - 1\right)^{1.67} \cdot \sqrt{g} \cdot D_{50}^{1.5} \cdot S^{-1.12}; \tag{A23}$$

ESURFD
2, 733–772, 2014

A7 Fractional bedload capacity estimation according to Rickenmann (2001) based on θ

$$\Phi_{\mathrm{bi}} = 3.1 \cdot \left(\frac{D_{90}}{D_{30}}\right)^{0.2} \cdot \sqrt{\theta_{i,\mathrm{r}}} \cdot \left(\theta_{i,\mathrm{r}} - \theta_{ci,\mathrm{r}}\right) \cdot \mathrm{Fr} \cdot \frac{1}{\sqrt{\frac{\rho_\mathrm{s}}{\rho} - 1}} \tag{A24}$$

$$\text{with} \quad \Phi_{\mathrm{bi}} = \frac{q_{\mathrm{bi}}}{F_i \sqrt{(\frac{\rho_\mathrm{s}}{\rho} - 1) g D_i^3}} \quad \text{and} \quad q_\mathrm{b} = \Sigma q_{\mathrm{bi}};$$

Acknowledgements. We are especially greatful to Christa Stephan (project thesis ETH/WSL), Lynn Burkhard (MSc thesis ETH/WSL) and Martin Böckli (WSL) for their contributions to the development of sedFlow. We highly appreciate the support of Alexandre Badoux (WSL), who helped us and revised the manuscript. We thank the Swiss National Science Foundation for funding of this work in the framework of the NRP 61 project "Sedriver" (SNF grant no. 4061-125975/1/2).

References

Badoux, A. and Rickenmann, D.: Berechnungen zum Geschiebetransport während der Hochwasser 1993 und 2000 im Wallis, Wasser Energie Luft, 100, 217–226, 2008. 742

Boyer, C., Verhaar, P. M., Roy, A. G., Biron, P. M., and Morin, J.: Impacts of environmental changes on the hydrology and sedimentary processes at the confluence of St. Lawrence tributaries: potential effects on fluvial ecosystems, Hydrobiologia, 647, 163–183, doi:10.1007/s10750-009-9927-1, 2010. 763

Carpentier, S., Konz, M., Fischer, R., Anagnostopoulos, G., Meusburger, K., and Schoeck, K.: Geophysical imaging of shallow subsurface topography and its implication for shallow landslide susceptibility in the Urseren Valley, Switzerland, J. Appl. Geophys., 83, 46–56, doi:10.1016/j.jappgeo.2012.05.001, 2012. 763

Cheng, N.-S.: Exponential formula for bedload transport, J. Hydraul. Eng.-ASCE, 128, 942–946, doi:10.1061/(ASCE)0733-9429(2002)128:10(942), 2002. 742, 754

Chiari, M. and Rickenmann, D.: Back-calculation of bedload transport in steep channel with a numerical model, Earth Surf. Proc. Land., 36, 805–815, doi:10.1002/esp.2108, 2011. 735, 742, 746, 763

Chiari, M., Friedl, K., and Rickenmann, D.: A one-dimensional bedload transport model for steep slopes, J. Hydraul. Res., 48, 152–160, doi:10.1080/00221681003704087, 2010. 735, 738, 763

Chow, V. T., Maidment, D. R., and Mays, L. W.: Applied Hydrology, McGraw-Hill, New York, 1988. 738

Ciarapica, L. and Todini, E.: TOPKAPI: a model for the representation of the rainfall–runoff process at different scales, Hydrol. Process., 16, 207–229, doi:10.1002/hyp.342, 2002. 736

Cui, Y. and Parker, G.: Numerical Model of Sediment Pulses and Sediment-Supply Disturbances in Mountain Rivers, J. Hydraul. Eng.-ASCE, 131, 646–656, doi:10.1061/(ASCE)0733-9429(2005)131:8(646), 2005. 735

Cui, Y. and Wilcox, A.: Development and application of numerical models of sediment transport associated with dam removal, in: Sedimentation Engineering – Processes, Measurements, Modeling and Practice, edited by: García, M. H., vol. 110 of ASCE Manual and Reports on Engineering Practice, American Society of Civil Engineers (ASCE), Reston, USA, chap. 23, 995–1020, doi:10.1061/9780784408148.ch23, 2008. 735

Cui, Y., Parker, G., Braudrick, C., Dietrich, W. E., and Cluer, B.: Dam Removal Express Assessment Models (DREAM). Part 1: Model development and validation, J. Hydraul. Res., 44, 291–307, doi:10.1080/00221686.2006.9521683, 2006. 734

Danish Hydraulic Institute (DHI): MIKE21C user's guide and scientific documentation, Tech. rep., DHI, Horsholm, Denmark, 1999. 735

Ferguson, R. I.: Flow resistance equations for gravel- and boulder-bed streams, Water Resour. Res., 43, W05427, doi:10.1029/2006WR005422, 2007. 741

Ferguson, R. I., Church, M., and Weatherly, H.: Fluvial aggradation in Vedder River: testing a one-dimensional sedimentation model, Water Resour. Res., 37, 3331–3347, doi:10.1029/2001WR000225, 2001. 763

Fernandez Luque, R. and van Beek, R.: Erosion and transport of bed-load sediment, J. Hydraul. Res., 14, 127–144, 1976. 743

García-Martinez, R., Espinoza, R., Valeraa, E., and González, M.: An explicit two-dimensional finite element model to simulate short- and long-term bed evolution in alluvial rivers, J. Hydraul. Res., 44, 755–766, doi:10.1080/00221686.2006.9521726, 2006. 735

ESURFD
2, 733–772, 2014

Heimann, F. U. M., Rickenmann, D., Böckli, M., Badoux, A., Turowski, J. M., and Kirchner, J. W.: Recalculation of bedload transport observations in Swiss mountain rivers using the model sedFlow, Earth Surf. Dynam. Discuss., 2, 773–822, doi:10.5194/esurfd-2-773-2014, 2014. 734, 737, 740, 750, 753, 763

Hoey, T. B. and Ferguson, R. I.: Numerical simulation of downstream fining by selective transport in gravel bed rivers: model development and illustration, Water Resour. Res., 30, 2251–2260, doi:10.1029/94WR00556, 1994. 735, 763

Hoey, T. B., Bishop, P., and Ferguson, R. I.: Testing numerical models in geomorphology: how can we ensure critical use of model predictions?, in: Prediction in Geomorphology, edited by: Wilcock, P. R. and Iverson, R. M., Vol. 135 of Geophysical Monograph, American Geophysical Union, Washington DC, USA, 241–256, doi:10.1029/135GM17, 2003. 763

Hunziker, R. P.: Fraktionsweiser Geschiebetransport, in: Mitteilung der Versuchsanstalt für Wasserbau, Hydrologie und Glaziologie, edited: by Vischer, D., 138, ETH, Zurich, Switzerland, 1–209, 1995. 748

Jäggi, M. N. R.: Sedimenthaushalt und Stabilität von Flussbauten, in: Mitteilung der Versuchsanstalt für Wasserbau, Hydrologie und Glaziologie, edited by: Vischer, D., 119, ETH, Zurich, Switzerland, 1–105, 1992. 749

Junker, J., Heimann, F. U. M., Hauer, C., Turowski, J. M., Rickenmann, D., Zappa, M., and Peter, A.: Assessing the impact of climate change on brown trout (Salmo trutta fario) recruitment, Hydrobiologia, in revision, 2014. 763

Kaitna, R., Chiari, M., Kerschbaumer, M., Kapeller, H., Zlatic-Jugovic, J., Hengl, M., and Huebl, J.: Physical and numerical modelling of a bedload deposition area for an Alpine torrent, Nat. Hazards Earth Syst. Sci., 11, 1589–1597, doi:10.5194/nhess-11-1589-2011, 2011. 763

Konz, M., Chiari, M., Rimkus, S., Turowski, J. M., Molnar, P., Rickenmann, D., and Burlando, P.: Sediment transport modelling in a distributed physically based hydrological catchment model, Hydrol. Earth Syst. Sci., 15, 2821–2837, doi:10.5194/hess-15-2821-2011, 2011. 736, 763

Lamb, M. P., Dietrich, W. E., and Venditti, J. G.: Is the critical Shields stress for incipient sediment motion dependent on channel-bed slope?, J. Geophys. Res., 113, F02008, doi:10.1029/2007JF000831, 2008. 743

Li, S. S. and Millar, R. G.: Simulating bed-load transport in a complex gravel-bed river, J. Hydraul. Eng.-ASCE, 133, 323–328, doi:10.1061/(ASCE)0733-9429(2007)133:3(323), 2007. 735

Liu, Z. and Todini, E.: Towards a comprehensive physically-based rainfall-runoff model, Hydrol. Earth Syst. Sci., 6, 859–881, doi:10.5194/hess-6-859-2002, 2002. 739, 741, 746, 752

Lopez, J. L. and Falcon, M. A.: Calculation of bed changes in mountain streams, J. Hydraul. Eng.-ASCE, 125, 263–270, doi:10.1061/(ASCE)0733-9429(1999)125:3(263), 1999. 735, 750

Meyer-Peter, E. and Müller, R.: Formulas for bed-load transport, in: Proceedings of the 2nd Meeting of the International Association for Hydraulic Structures Research, Appendix 2, Stockholm, Sweden, 7–9 June 1948, 1948. 743

Morvan, H., Knight, D., Wright, N., Tang, X., and Crossley, A.: The concept of roughness in fluvial hydraulics and its formulation in 1D, 2D and 3D numerical simulation models, J. Hydraul. Res., 46, 191–208, doi:10.1080/00221686.2008.9521855, 2008. 742

Mouri, G., Shiiba, M., Hori, T., and Oki, T.: Modeling reservoir sedimentation associated with an extreme flood and sediment flux in a mountainous granitoid catchment, Japan, Geomorphology, 125, 263–270, doi:10.1016/j.geomorph.2010.09.026, 2011. 735

Nitsche, M., Rickenmann, D., Turowski, J. M., Badoux, A., and Kirchner, J. W.: Evaluation of bedload transport predictions using flow resistance equations to account for macro-roughness in steep mountain streams, Water Resour. Res., 47, W08513, doi:10.1029/2011WR010645, 2011. 734, 742, 743, 745

Nitsche, M., Rickenmann, D., Kirchner, J. W., Turowski, J. M., and Badoux, A.: Macroroughness and variations in reach-averaged flow resistance in steep mountain streams, Water Resour. Res., 48, W12518, doi:10.1029/2012WR012091, 2012. 734, 742

Papanicolaou, A. N., Bdour, A., and Wicklein, E.: One-dimensional hydrodynamic/sediment transport model applicable to steep mountain streams, J. Hydraul. Res., 42, 357–375, doi:10.1080/00221686.2004.9641204, 2004. 735

Parker, G.: Transport of gravel and sediment mixtures, in: Sedimentation Engineering: Processes, Measurements, Modeling, and Practice, Vol. 110 of ASCE Manuals and Reports on Engineering Practice, American Society of Civil Engineers (ASCE), Chap. 3, 165–252, Reston, VA, USA, 2008. 744, 746

Recking, A.: Theoretical development on the effects of changing flow hydraulics on incipient bed load motion, Water Resour. Res., 45, W04401, doi:10.1029/2008WR006826, 2009. 745

ESURFD
2, 733–772, 2014

Recking, A.: A comparison between flume and field bed load transport data and consequences for surface-based bed load transport prediction, Water Resour. Res., 46, W03518, doi:10.1029/2009WR008007, 2010. 743, 755
Rickenmann, D.: Comparison of bed load transport in torrent and gravel bed streams, Water Resour. Res., 37, 3295–3305, doi:10.1029/2001WR000319, 2001. 742, 743, 756, 757
Rickenmann, D.: Alluvial steep channels: flow resistance, bedload transport prediction, and transition to debris flows, in: Gravel-bed Rivers: Processes, Tools, Environments, edited by: Church, M., Biron, P. M., and Roy, A. G., John Wiley & Sons, 386–397, Chichester, UK, 2012. 742
Rickenmann, D. and Recking, A.: Evaluation of flow resistance in gravel-bed rivers through a large field data set, Water Resour. Res., 47, W07538, doi:10.1029/2010WR009793, 2011. 734, 741, 742
Shields, A.: Anwendung der Aehnlichkeitsmechanik und der Turbulenzforschung auf die Geschiebebewegung, Tech. rep., Mitteilungen der Preussischen Versuchsanstalt für Wasserbau und Schiffbau, Berlin, 1936. 743
Soulsby, R. L. and Damgaard, J. S.: Bedload sediment transport in coastal waters, Coast. Eng., 52, 673–689, doi:10.1016/j.coastaleng.2005.04.003, 2005. 743
Stephan, C.: Sensitivity of bedload transport simulations to different transport formulae and cross-sectional geometry with the model Tom^{Sed}, Tech. rep., Swiss Federal Research Institute WSL & ETH, Zurich, 2012. 746, 747, 768
Sternberg, H.: Untersuchungen über Längen- und Querprofil geschiebeführender Flüsse, Zeitschrift für Bauwesen, 25, 483–506, 1875. 744
Talbot, T. and Lapointe, M.: Numerical modeling of gravel bed river response to meander straightening: the coupling between the evolution of bed pavement and long profile, Water Resour. Res., 38, 10-1–10-10, doi:10.1029/2001WR000330, 2002. 763
van de Wiel, M. J., Coulthard, T. J., Macklin, M. G., and Lewin, J.: Embedding reach-scale fluvial dynamics within the CAESAR cellular automaton landscape evolution model, Geomorphology, 90, 283–301, doi:10.1016/j.geomorph.2006.10.024, 2007. 738, 747, 748
Verhaar, P. M., Biron, P. M., Ferguson, R. I., and Hoey, T. B.: A modified morphodynamic model for investigating the response of rivers to short-term climate change, Geomorphology, 101, 674–682, doi:10.1016/j.geomorph.2008.03.010, 2008. 735, 763

ESURFD
2, 733–772, 2014

Wilcock, P. R. and Crowe, J. C.: Surface-based transport model for mixed-size sediment, J. Hydraul. Eng.-ASCE, 129, 120–128, doi:10.1061/(ASCE)0733-9429(2003)129:2(120), 2003. 743, 744, 745, 754, 765

Yager, E. M., Kirchner, J. W., and Dietrich, W. E.: Calculating bed load transport in steep boulder bed channels, Water Resour. Res., 43, W07418, doi:10.1029/2006WR005432, 2007. 742

Yager, E. M., Dietrich, W. E., Kirchner, J. W., and McArdell, B. W.: Prediction of sediment transport in step-pool channels, Water Resour. Res., 48, W01541, doi:10.1029/2011WR010829, 2012. 742

ESURFD

2, 733–772, 2014

Table 1. Comparison of bedload transport models for steep mountain streams. The information on calculation speed refer to the simulation of a 20 km long study reach of a regular mountain river.

	Topkapi ETH	Tom^{Sed}	SEDROUT	sedFlow
main aims	integral simulation of different processes at different scales featuring spatial and temporal subgridding	simulation of the effect of the shape of channel cross-sections on bedload transport featuring a user defined, detailed channel geometry	detailed simulation of the spatial and temporal evolution of local grain size distributions; river bifurcations	fractional transport; consideration of adverse slopes; fast simulations and straightforward pre- and postprocessing of simulation data
speed	simulation of several days within few minutes of computation time	slightly faster than real time		simulation of several years within few hours of computation time
input format	partially *Matlab* preprocessing required	xml files		mainly regular spreadsheets
intended applications	mainly scientific	engineering and scientific	mainly scientific	mainly engineering and operational
references	Konz et al. (2011), Carpentier et al. (2012)	Chiari et al. (2010); Chiari and Rickenmann (2011); Kaitna et al. (2011)	Hoey and Ferguson (1994); Ferguson et al. (2001); Talbot and Lapointe (2002); Hoey et al. (2003); Verhaar et al. (2008); Boyer et al. (2010)	Junker et al. (2014), Heimann et al. (2014)

ESURFD
2, 733–772, 2014

Table A1. Notation.

The following symbols are used in this article:	
∇	= nabla operator
β	= an empiric constant factor
γ	= correction factor for θ_{ci}
Δt	= temporal discretisation i.e. time step duration
Δx	= spatial discretisation i.e. reach length
ΔX	= travel distance of grains
η_{pore}	= pore volume fraction
θ	= dimensionless bed shear stress
θ_{50}	= representative θ for D_{50}
θ_c	= dimensionless bed shear stress threshold for initiation of bedload motion
θ_{ca}	= representative θ_c for the active layer
θ_{ci}	= θ_c for ith grain size fraction
$\theta_{ci,\text{r}}$	= θ_{ci} corrected for form roughness
θ_{cs}	= representative θ_c for the subsurface alluvium
θ_{c84}	= θ_c for D_{84}
θ_i	= θ for ith grain size fraction
$\theta_{i,\text{r}}$	= θ_i corrected for form roughness
λ	= empiric abrasion coefficient
μ	= dynamic viscosity
ρ	= fluid density
ρ_{s}	= sediment density
τ	= bed shear stress
τ_{r}	= reference bed shear stress
τ_{rm}	= reference bed shear stress of mean size of bed surface
τ^*_{rm}	= reference dimensionless Shields stress for mean size of bed surface
Φ_{b}	= dimensionless bedload flux
A	= wetted cross-sectional area
a,b,d	= empiric constants
D	= grain diameter
D_i	= mean grain diameter for ith grain size fraction
D_{m}	= geometric mean for grain diameters
D_{mArith}	= arithmetic mean for grain diameters
$D_{\text{mArith}_{\text{a}}}$	= D_{mArith} for the active layer
$D_{\text{mArith}_{\text{s}}}$	= D_{mArith} for the subsurface alluvium
D_x	= xth percentile for grain diameters
D_{xsurf}	= xth percentile for grain diameters of bed surface
D_{50}	= median grain diameter
e	= empiric constant ranging from 1 to 2
exp	= exponential function
$\boldsymbol{f}$	= body forces
f	= Darcy–Weisbach friction factor
F_i	= proportion of ith grain size fraction

ESURFD
2, 733–772, 2014

Table A1. Continued.

fr	= flow resistance
Fr	= Froude number
g	= gravitational acceleration
geom	= channel geometry
i_s	= grain size influence from the subsurface alluvium
j_1, j_2, k, l	= empiric constants
L	= process break point
m	= empiric hiding exponent
m_{wc}	= hiding exponent according to Wilcock and Crowe (2003)
p	= pressure
q	= discharge per unit flow width
q_b	= bedload flux per unit flow width
$q_{b_{abr}}$	= q_b corrected for gravel abrasion
$q_{b_{lat}}$	= lateral bedload influx per unit flow width
q_c	= threshold discharge per unit flow width for initiation of bedload motion
Q	= discharge
Q_c	= threshold Q for the initiation of bedload motion
Q_{max}	= maximum Q for the simulation period
Q_{rep}	= representative Q for the simulation period
Q_{lat}	= lateral water influx
r_h	= hydraulic radius
$r_{h,c}$	= r_h for $[\theta_{50} = \theta_c]$
s	= density ratio of solids and fluids
S	= slope
S_b	= channel bed slope
S_c	= virtual slope for the correction of θ_{ci} based on $r_{h,c}$
S_f	= friction slope
S_{red}	= slope reduced for form roughness
t	= time
$_T$	= of current time step
$_{T-1}$	= of previous time step
$_u$	= of upstream river reach
$\boldsymbol{v}$	= flow velocity vector
v	= flow velocity scalar
v^*	= shear velocity
V	= water volume in reach
w	= channel width
W^*	= dimensionless bedload transport rate
x	= distance in flow direction
z	= elevation of channel bed

ESURFD
2, 733–772, 2014

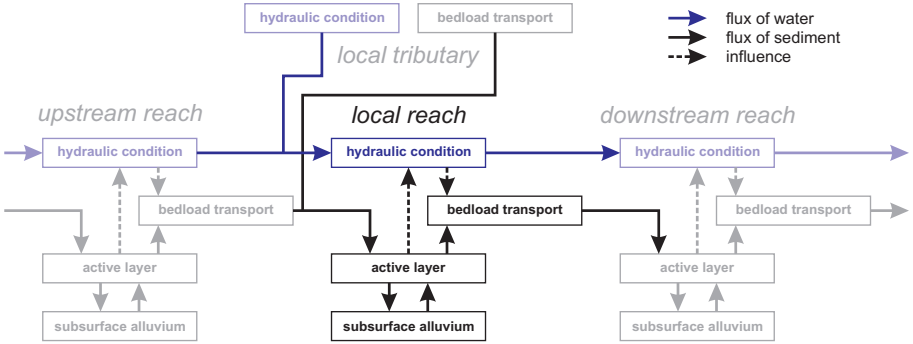

Figure 1. Overview over the main process interactions within the sedFlow model.

ESURFD
2, 733–772, 2014

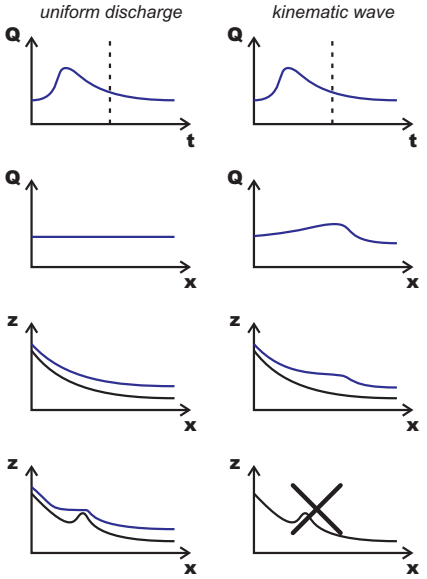

Figure 2. Qualitative comparison of uniform discharge (left) and kinematic wave (right) flow routing approaches. The top row shows a hypothetical discharge time series at the upstream boundary, which can be used in both approaches. The point in time for the following rows is indicated by the dashed vertical line. In the uniform discharge approach, the current discharge value of the time series defines the discharge for all reaches of the simulated system at the current point in time (second row left). In contrast, for the kinematic wave approach, the temporal variability of discharge is reflected in a spatial variability as well (second row right). Therefore in the uniform discharge approach, the spatial variation of flow depth (third row) and thus water surface (blue curve) is mainly a function of roughness and slope, which is determined by the river bed (black curve). For the kinematic wave approach, flow depth may also vary due to the spatial variation of discharge (third row right). In cases of adverse bed slopes, the uniform discharge approach will reproduce the effects of ponding (fourth row left), while the kinematic wave approach cannot deal with such situations (fourth row right).

ESURFD
2, 733–772, 2014

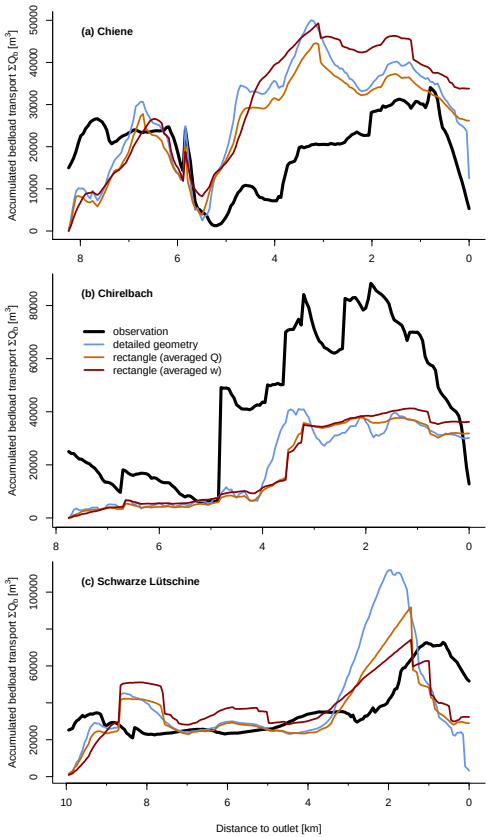

Figure 3. Comparison of the effects of different channel representations on accumulated bedload transport estimates simulated with the Tom^{Sed} model. See text and Stephan (2012) for details.

ESURFD
2, 733–772, 2014

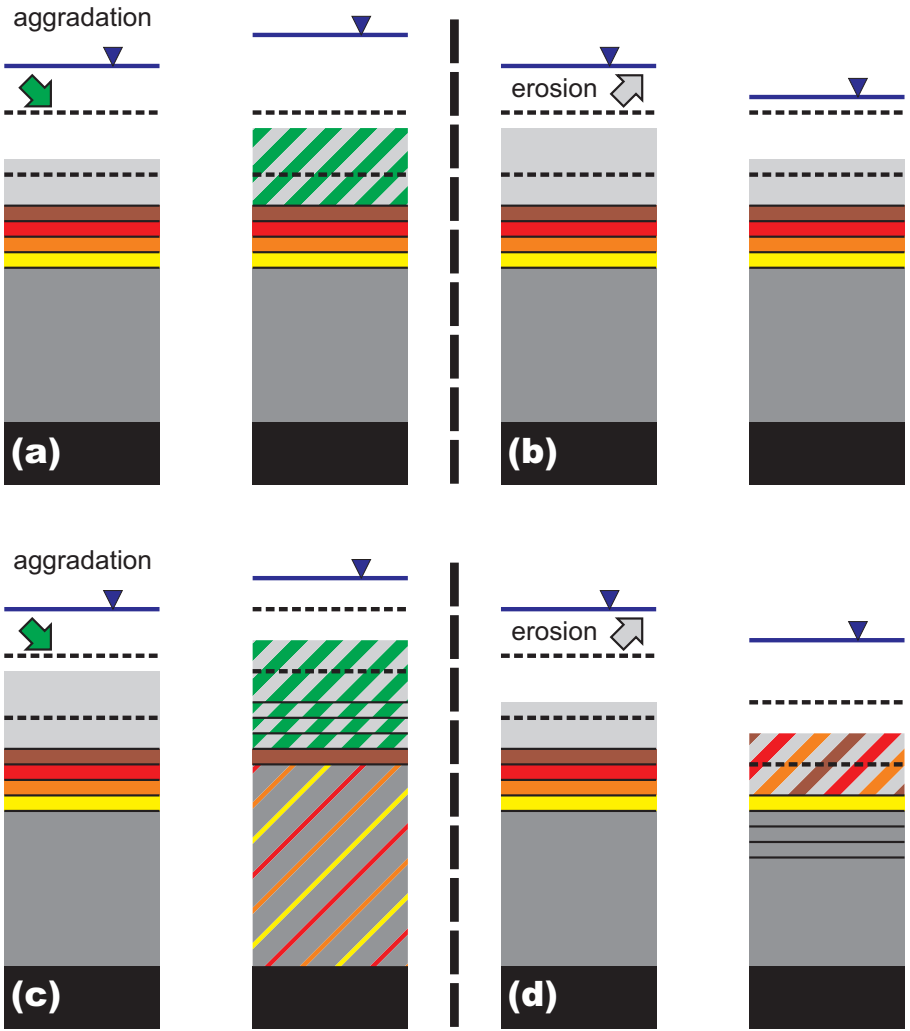

ESURFD
2, 733–772, 2014

Figure 4. Qualitative sketch of threshold-based interaction between active layer and subsurface alluvium. The water level is displayed in blue, the active layer with its variable thickness is light grey and bed rock is black. The subsurface alluvium consists of several strata layers with user defined constant thickness displayed in reddish colours and one base layer with variable thickness displayed in dark grey. The horizontal dashed lines indicate the thresholds for the thickness of the active layer. In case of aggradation (**a** and **c**), the material input from upstream, which is displayed in green, is added to the active layer, which is instantaneously homogenised. Any homogenisation process is displayed by diagonal stripes. If the thickness of the active layer does not exceed its thresholds after aggradation or erosion (**a** and **b**) the thresholds of the active layer and the layers of the subsurface alluvium remain constant. If the active layer thickness exceeds its upper threshold after aggradation **(c)**, the complete system of layers and thresholds is shifted upwards so that the thickness of the active layer is in the middle between its thresholds. The upper strata layers are populated with material from the homogenised active layer, while the material of the lower strata layers is added to the base layer, which is instantaneously homogenised. If the active layer thickness exceeds its lower threshold after erosion **(d)**, the complete system of layers and thresholds is shifted downwards so that the thickness of the active layer is in the middle between its thresholds. The lower strata layers are populated with material from the base layer, while the material of the upper strata layers is added to the active layer, which is instantaneously homogenised.

ESURFD
2, 733–772, 2014

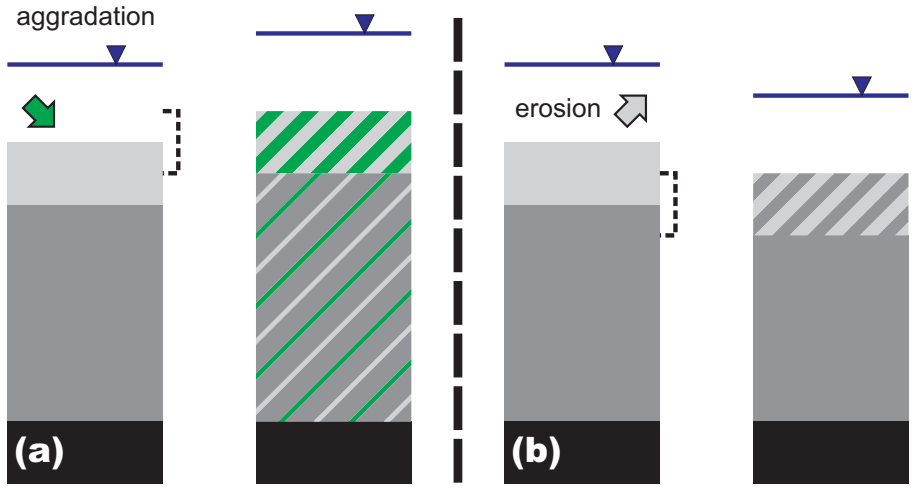

Figure 5. Qualitative sketch of continuous interaction between active layer and subsurface alluvium. The water level is displayed in blue, the active layer with its constant thickness is light grey, the subsurface alluvium consisting of one layer with variable thickness is dark grey and bed rock is black. The dashed bracket indicates the position of the active layer after aggradation or erosion. In case of aggradation **(a)**, the material input from upstream, which is displayed in green, is added to the active layer, which is instantaneously homogenised. Any material of the homogenised active layer, which exceeds the constant thickness, is transferred to the subsurface alluvium, which is instantaneously homogenised as well. Any homogenisation process is displayed by diagonal stripes. In case of erosion **(b)**, the sediment deficit of the active layer is replaced from the subsurface alluvium and the active layer is instantaneously homogenised.

ESURFD
2, 733–772, 2014

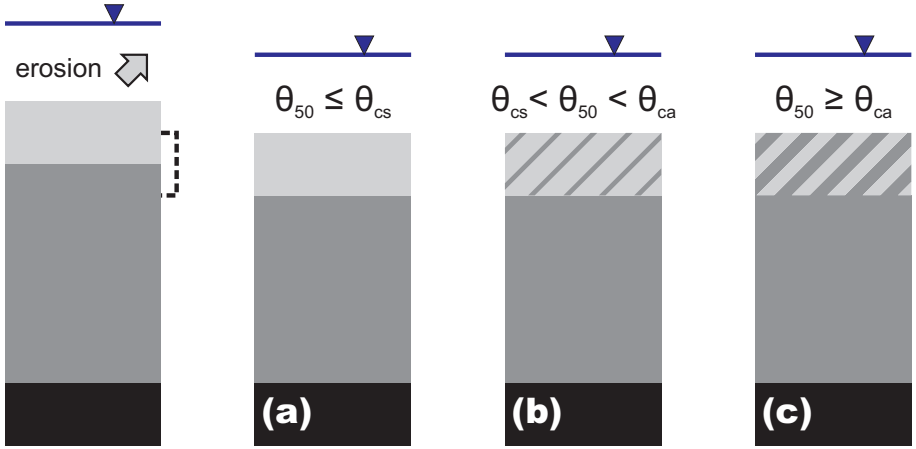

Figure 6. Qualitative sketch of shear-stress-based interaction between active layer and subsurface alluvium. For explanation of the symbols see the caption of Fig. 5. In this approach, the aggradation case is treated identically to the continuous update approach displayed in Fig. 5a. For erosion, three cases are differentiated, with the representative dimensionless shear stress θ_{50} increasing from case a to case c. If θ_{50} equals or exceeds the threshold for the active layer θ_{ca} **(c)**, the layers interact in the same way as in the continuous update approach displayed in Fig. 5b. If θ_{50} does not exceed the threshold for the subsurface alluvium θ_{cs} **(a)**, the volume deficit of the active layer is replaced from the subsurface alluvium, but the grain size distribution of the active layer remains constant. For the intermediate case with θ_{50} greater than θ_{cs} and smaller than θ_{ca} **(b)**, the influence of the grain size distribution of the subsurface alluvium on the grain size distribution of the active layer is interpolated linearly between cases a and c.

ESURFD
2, 733–772, 2014